Crystal Growth of Quaternary $RE_2EuSi_2S_8$ (*RE* = Ce - Nd, Sm, Gd, Tb) Using Flux-Assisted Boron Chalcogen Mixture (BCM) Method: Investigation of Magnetic and Luminescence Properties

Habiba Binte Kashem[1], Hope Smith[1], Md Abdullah Al Muhit[1], and Hans-Conrad zur Loye[1*]

[1]Department of Chemistry and Biochemistry, University of South Carolina, Columbia, SC, 29208, United States

*E-mail: zurloye@mailbox.sc.edu

Abstract:

A series of quaternary rare-earth containing thiosilicates with the general formula $RE_2EuSi_2S_8$ (*RE* = Ce - Nd, Sm, Gd, Tb) has been synthesized via the flux-assisted boron chalcogen mixture (BCM) crystal growth method. High-quality single crystals were obtained, and their crystal structures were determined by single-crystal X-ray diffraction. The $RE_2EuSi_2S_8$ series crystallizes in the trigonal system, adopting the space group *R*-3*c*. Polycrystalline samples were employed for physical property measurements, including magnetic susceptibility measurements, UV-visible diffuse reflectance, and photoluminescent response. Magnetic data of $RE_2EuSi_2S_8$ (*RE* = Ce, Nd, and Gd) were collected over the 2 – 300 K temperature range. The samples are paramagnetic behavior with negative Weiss constants (θ_W = -11.05, -10.55, and -1.35 K respectively). Their thermal stability was investigated using thermogravimetric analysis (TGA). Optical band gaps, estimated from diffuse reflectance spectra, were determined to be 2.2(1) eV for $Ce_2EuSi_2S_8$, 1.8(1) eV for $Nd_2EuSi_2S_8$, and 1.7(1) eV for $Gd_2EuSi_2S_8$ respectively. Photoluminescence measurements were collected on $Ce_2EuSi_2S_8$, and $Tb_2EuSi_2S_8$ single crystals.

Introduction:

The development of new compounds with increasingly complex composition, such as ternary and quaternary phases, has become a major direction of modern material science as it is thought to potentially lead to new or perhaps improved physical properties. Among these multi-component systems, complex metal chalcogenides occupy an important position due to their wide-ranging physical properties along with rich structural diversity.[1-3] In fact, rare-earth metal containing complex chalcogenides have attracted significant interest due to their distinctive thermal,[4] magnetic,[5] photovoltaic,[6] and optical properties, which make them promising candidates for applications in infrared technologies, optoelectronics,[7] photoluminescence,[8] scintillation,[9] and nonlinear optics.[10]

The luminescent behavior of metal chalcogenides has drawn considerable attention owing to their potential in LED lighting, and display technologies.[11-13] One strategy for designing new luminescent materials is the incorporation of suitable luminophores into a well-defined crystal framework.[14] Over the past several decades, the luminescent behavior of binary, ternary, and quaternary sulfides have been studied by introducing transition metal or rare-earth metal dopants into selected host structures,[15-19] where the dopant ions can either partially or fully occupy crystallographic sites. Therefore, the synthesis and structural characterization of luminescent chalcogenide materials is of considerable interest in the search of new luminescent compounds.

While the considerable application potential of these materials makes them highly desirable, their synthesis is made extremely challenging by the high moisture and oxygen sensitivity of the rare earth metals. In addition, the limited availability of commercial sources of binary rare-earth chalcogenides makes it necessary to prepare such reactants prior to exploring the synthesis of the target compounds. This issue has been addressed in the zur Loye group by using the boron chalcogen mixture (BCM) method, which was first implemented by Wu and Seo to synthesize the binary metal chalcogenides.[20] The BCM method offers a convenient pathway for preparing mixed-metal chalcogenides from metal oxide precursors and the zur Loye group has recently extended this method to the synthesis of actinide and lanthanide containing chalcogenides.[21-23] The BCM method yields different ternary and quaternary chalcogenides, enabling reliable structural and physical property measurements including thermoelectric application,[24] magnetic behavior,[25] second harmonic generation (SHG) measurement[26] etc.

Although numerous series of thiosilicates have been reported, their remarkable structural flexibility leaves significant room for exploring new structural compositions.[23, 27] During the synthesis of $Ce_{1.97}Eu_{1.03}Ag_{0.06}SiS_7$[28], a minor secondary phase was detected and identified by single crystal X-ray diffraction as $Ce_2EuSi_2S_8$, a member of the $Eu_3(AsS_4)_2$ family.[29] The intriguing characteristics reported for these family motivated us to explore this series more extensively.[13, 30-32] All the previously known members of this family were synthesized by solid-state synthesis via the sintering of elemental precursors at elevated temperatures. Recently the zur Loye group has reported A$RE_2Si_2S_8$ (A = Ca, Sr; *RE* = La - Tb) by using the molten flux assisted BCM method.[33] The molten flux synthesis has also been extensively used in the zur Loye group for the crystal growth of a wide variety of compounds.[27, 34, 35] Therefore, we decided to employ the BCM method along with the molten flux and solid-state techniques for the synthesis and crystal growth of $RE_2EuSi_2S_8$ compounds.

In this work, we present the crystal growth of high-quality single crystals of $RE_2EuSi_2S_8$ (*RE* = Ce - Nd, Sm, Gd, Tb), their single-crystal structural characterization, and investigation of their optical, magnetic properties across selected members of the series.

Experimental Section:

RE_2O_3 (*RE* = Nd, Sm, Eu, Gd) (99.9%, Alfa Aesar), CeO_2 (99.9%, Alfa Aesar), Pr_6O_{11} (99.9% Alfa Aesar), Tb_4O_7 (99.9% Alfa Aesar), sulfur powder (99.5% Fisher Scientific), boron (crystalline 100 mesh, 99.9%, Beantown Chemical), AgI (99%, Thermo Scientific), sodium thiosulfate pentahydrate (high purity grade, VWR Chemicals) reagents were used as received for the synthesis of the targeted compounds.

$RE_2EuSi_2S_8$ (*RE* = Ce – Nd, Sm, Gd, Tb) single crystals were synthesized by the addition of the starting reagents, RE_2O_3 (*RE* = Nd, Sm, Gd)/ CeO_2/ Pr_6O_{11}/ Tb_4O_7, Eu_2O_3, SiO_2, B, S powders in a 1 (2 for CeO_2, 0.333 for Pr_6O_{11}, 0.5 for Tb_4O_7):1:2:15:20 molar ratio. A total weight of 250 mg of the starting reagents was placed into a heavily carbon coated fused silica tube along with 250 mg AgI. The fused silica tube was evacuated to 10^{-4} torr and flame-sealed using a methane/oxygen torch. The sealed fused silica tube was placed into a programmable furnace, heated to 850 °C in 10 h, dwell at this temperature for 36 h, and cooled to 300 °C in 36 h, at which point the furnace was shut off and the tubes were allowed to cool down to room temperature. The tubes were then cut open, and the resulting products were washed with ~3M sodium thiosulfate

solution for the removal of the AgI flux. All the products exhibited reasonable air and moisture stability.

Washing the samples with sodium thiosulfate solution removed all the residual AgI flux, resulting in an almost phase-pure powder with only trace impurities for $RE_2EuSi_2S_8$ (*RE* = Ce, and Nd), Figures S1-S2. However, $RE_2EuSi_2S_8$ (*RE* = Pr, Sm, Gd, Tb) did not give phase pure sample. To target phase pure powder of $RE_2EuSi_2S_8$ (*RE* = Pr, Sm, Gd, Tb), solid-state synthesis along with the BCM method was performed by reacting RE_2O_3 (*RE* = Sm, Gd)/ Pr_6O_{11}/ Tb_4O_7, Eu_2O_3, SiO_2, B, S powders in a 1 (0.333 for Pr_6O_{11}, 0.5 for Tb_4O_7):0.5:2:6:8 molar ratio in the absence of AgI. However, we were unable to obtain a phase-pure product, although several attempts were made using different reaction condition. In every attempt, inevitable binary RE_2S_3 phase for Sm, Gd, Tb analogues formed along with our target phase, Figures S3-S5. Unfortunately for the Pr analogue we could not obtain the target phase. The powder X-ray diffraction analysis confirms the phase purity of the samples that were used for further property measurements.

Caution. *Boron sulfides can cause the generation of H_2S gas upon contact with moisture and water due to their moisture-sensitivity. Therefore, all reaction work should be conducted in a fume hood, following proper safety protocols.*

Single-Crystal X-ray Diffraction (SXRD).

Single-crystal X-ray diffraction data of the $RE_2EuSi_2S_8$ (*RE* = Ce – Nd, Sm, Gd, Tb) series were collected at room temperature on a Bruker D8 QUEST diffractometer equipped with a PHOTON-II area detector and an Incoatec microfocus radiation source (Mo Kα radiation, λ = 0.71073 Å). The suitable sized single crystals were mounted on a microloop by using immersion oil. An exposure time of 10 s/frame was used for collecting the data while the distance from the detector to crystal was fixed to 40 mm. the SAINT and SADABS programs were used for performing the reduction and absorption correction of the raw data.[36] An initial structural model was obtained with SHELXT. Full-matrix least-squares refinements against $|F|^2$ were performed with the SHELXL software[37] using the Olex2 interface.[38] The detailed crystallographic data and diffraction results are provided in Table 1. All compounds crystallize in the trigonal crystal system with the space group *R*-3*c*. All atoms were refined with anisotropic displacement parameters, and the asymmetric unit contains four independent atomic positions, one occupied by *RE* (*RE* = Ce – Nd, Sm, Gd, Tb), and Eu exhibiting anti-site mixing, one occupied by Si, and two occupied by S.

Powder X-ray Diffraction (PXRD).

Powder X-ray diffraction (PXRD) patterns were obtained using finely ground polycrystalline samples of $RE_2EuSi_2S_8$ prepared by the solid-state synthesis BCM method (Figures S1-S5). PXRD data were collected on a Bruker D2 PHASER diffractometer over the 2θ range 5−65° with a step size of 0.02° with Cu−Kα radiation (λ = 1.5418 Å).

Energy-Dispersive X-ray Spectroscopy (EDS).

Elemental analysis of single crystals was carried out using Energy-Dispersive X-ray Spectroscopy (EDS). For data collection, single crystals were mounted directly onto a SEM stub with carbon tape. Quantitative elemental analysis was performed with a TESCAN Vega-3 SBU scanning electron microscope (SEM) equipped with a Thermo EDS attachment, operated in low vacuum mode. An accelerating voltage of 15-20 kV and accumulation time of 40 s were used. The summarized results are provided in the Supporting Information.

Magnetic Susceptibility.

Susceptibility and magnetization measurements of $RE_2EuSi_2S_8$ (*RE* = Ce, Nd, and Gd) were performed using a Quantum Design magnetic property measurement system (QD MPMS 3 SQUID Magnetometer). The magnetic susceptibility was measured under zero-field-cooled (ZFC) and field-cooled (FC) conditions from 2 to 300 K using an applied field of 0.1 T. Magnetization measurements were performed at 2 K by cycling the applied field from -5 to 5 T for $Ce_2EuSi_2S_8$, $Nd_2EuSi_2S_8$, and -7 to 7 T for $Gd_2EuSi_2S_8$. Data were corrected for the sample shape and radial offset effects as described previously.[39]

Thermogravimetric Analysis (TGA).

TGA was performed on polycrystalline samples using a SDT Q600 thermogravimetric analyzer. The samples were placed in alumina pans and heated from room temperature to 900 °C at a rate of 10 °C/min under a nitrogen flow of 100 mL/min. Following the TGA experiments, the resulting powders were further analyzed by PXRD for phase identification.

UV-vis Spectroscopy.

UV−vis diffuse reflectance spectra for $RE_2EuSi_2S_8$ (*RE* = Ce, Nd, and Gd) were obtained using a PerkinElmer Lambda 35 UV−vis spectrophotometer equipped with an integrating sphere.

Spectra were recorded over the 200-900 nm range at room temperature. The conversion of the reflectance data to absorbance was performed using the Kubelka-Munk function.[40]

Photoluminescence Emission Spectroscopy.

Photoluminescence data for $RE_2EuSi_2S_8$ (*RE* = Ce, and Tb) were collected using a HORIBA scientific standard microscope spectroscopy system using individual single crystals of $RE_2EuSi_2S_8$ (*RE* = Ce, and Tb). The system was outfitted with a HORIBA iHR320 imaging spectrograph and a CCD detector. A 375 nm diode laser source was used as the excitation source confocal. A laser excitation source of 10.0 mW and a 10X UV objective were used for data acquisition by using Labspec 6 in the 400 – 800 nm range.

Table 1. Crystallographic Data and Diffraction Results for $RE_2EuSi_2S_8$ Compounds

Chemical formula	**$Ce_2EuSi_2S_8$**	**$Pr_2EuSi_2S_8$**	**$Nd_2EuSi_2S_8$**	**$Sm_2EuSi_2S_8$**	**$Gd_2EuSi_2S_8$**	**$Tb_2EuSi_2S_8$**
Formula weight	744.74	746.33	753.02	765.30	779.17	782.53
Crystal system	Trigonal					
Space group	*R*-3*c*					
Temperature (K)	298.98	298.08	298.51	298.03	298.00	298.44
***a* (Å)**	9.01130(10)	8.97820(10)	8.95020(10)	8.9088(7)	8.87630(10)	8.86646(17)
c (Å)	26.7680(6)	26.6370(6)	26.5306(7)	26.349(4)	26.1774(8)	26.1044(8)
***V* (Å^3)**	1882.44(6)	1859.49(6)	1840.53(6)	1811.1(4)	1786.16(7)	1777.24(9)
Z	6					
μ (mm^{-1})	13.525	14.211	14.881	16.255	17.765	18.601
Crystal size (mm)	0.06 × 0.04 × 0.03	0.04 × 0.03 × 0.01	0.04 × 0.02 × 0.01	0.05 × 0.02× 0.02	0.04 × 0.03 × 0.01	0.05 × 0.04 × 0.02
ρ_{calcd} (g/cm^3)	3.942	3.999	4.076	4.210	4.346	4.387
Radiation (λ, Å)	Mo Kα (λ = 0.71073)					
2θ range, deg	6.044 – 72.616	6.068 – 72.722	6.088 – 72.85	6.12 – 72.698	6.146 – 72.678	6.156 – 72.754
Reflections collected	32451	32257	32069	35567	31040	30814
R_{int}	0.0314	0.0352	0.0354	0.0328	0.0401	0.0303
GOF (F^2)	1.152	1.137	1.094	1.067	1.126	1.064
R_1 ($I > 2\sigma(I)$)	0.0114	0.0113	0.0120	0.0134	0.0186	0.0195

wR_2 (all data)	0.0273	0.0261	0.0273	0.0301	0.0381	0.0417
$\Delta\rho_{max}$, $\Delta\rho_{min}$ (e Å^{-3})	0.78/-0.58	0.79/-0.66	0.78/-0.71	1.18/-1.11	1.57/-1.52	1.79/-1.77

Results and Discussions:

Synthesis:

A number of fluxes have been used for the preparation of chalcogenide phases, in particular fluxes that have some covalent character, such as NaI.[41] Using this flux we pursued the preparation of $Ce_{1.97}Eu_{1.03}Ag_{0.06}SiS_7$,[28] and observed a secondary phase that we identified by single crystal X-ray diffraction as $Ce_2EuSi_2S_8$. Our group had previously investigated the related series $ARE_2Si_2S_8$ (A = Ca, Sr; *RE* = La - Tb), which can be related to the title compounds via the replacement of the divalent alkaline earth metal with the divalent europium. Due to this similarity and also because europium in chalcogenides is typically found in the +2 oxidation state, we pursued the synthesis of this phase systematically via the BCM method. RE_2O_3 (*RE* = Nd, Sm, Gd)/ CeO_2/ Pr_6O_{11}/ Tb_4O_7, Eu_2O_3, SiO_2 were used as the *RE*, Eu, and Si sources respectively, and the boron served as oxygen scavenger for the oxide precursors, thus enabling them to react with elemental sulfur. AgI was used as the flux in this synthesis and could be readily removed post synthesis by dissolution in ~3M sodium thiosulfate. We attempted several reactions using different fluxes; however, we obtained our target phase only when using AgI as the flux.[41] Using AgI we successfully synthesized six new high-quality crystals of the $RE_2EuSi_2S_8$ series (*RE* = Ce, Pr, Nd, Sm, Gd, Tb), Figure 1. EDS elemental analyses confirmed that the crystals contain all of the expected elements (see Table S1) with no evidence of extraneous elemental impurities. Although we pursued the incorporation of lanthanides smaller than terbium, we were unsuccessful in obtaining these compositions. Therefore, we hypothesize that $Tb_2EuSi_2S_8$ marks the lower size limit for lanthanide incorporation into the $RE_2EuSi_2S_8$ series under our synthesis conditions. In addition, we were also unable to obtain $La_2EuSi_2S_8$, although several attempts were made using different heating profiles.

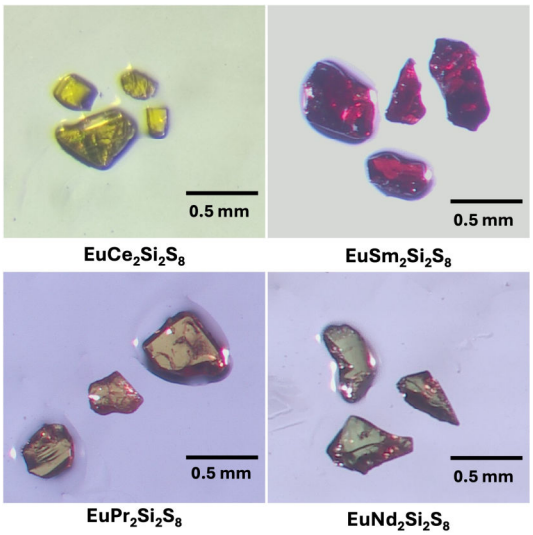

Figure 1: Optical images of crystals of $RE_2EuSi_2S_8$ (*RE* = Ce, Sm, Pr, and Nd)

The reaction products were washed with ~3M sodium thiosulfate solution to remove the AgI flux, and subsequently methanol was used to wash the products, resulting the almost phase pure samples (along with trace number of unidentified impurities) for $Ce_2EuSi_2S_8$, $Nd_2EuSi_2S_8$, Figure S1-S2. We attempted to prepare phase pure powder for $RE_2EuSi_2S_8$ (*RE* = Pr, Sm, Gd, Tb), via a BCM coupled solid state synthesis by reacting stoichiometric amounts of the starting reagents in the absence of a flux. Unfortunately, we were unable to obtain the completely phase pure samples. In the case of $Gd_2EuSi_2S_8$ only very minor Gd_2S_3 peaks were observed in the PXRD pattern, however, in the case of $RE_2EuSi_2S_8$ (*RE* = Sm, Tb) larger amounts of RE_2S_3 (*RE* = Sm, Tb) were observed, Figure S3-S5. Unfortunately, it was not possible to selectively dissolve the RE_2S_3 impurities to obtain entirely phase pure samples.

Crystal Structure

Figure 2 shows the three-dimensional structure of $Ce_2EuSi_2S_8$ structure as determined by the single crystal X-ray diffraction at room temperature. All synthesized $RE_2EuSi_2S_8$ (*RE* = Ce - Nd, Sm, Gd, and Tb) compositions crystallize in in the trigonal *R*-3*c* space group and are isostructural with the previously reported $ARE_2Si_2S_8$ (A = Ca, and Sr).[33, 42] The asymmetric unit cell contains four atomic sites, one mixed *RE*/Eu site, one Si site, and two S sites. It is important to note that, for each composition, refinement of the mixed-metal site occupancy yielded values of 0.656 to 0.667 for *RE*, and 0.343 to 0.333 for Eu, consistent with the ratio expected for charge balance. Therefore, in the final refinement for all $RE_2EuSi_2S_8$ (*RE* = Ce - Nd, Sm, Gd, and Tb)

compounds, the mixed-metal site occupancies were fixed at 2/3 *RE* and 1/3 Eu. The Si, and S sites are fully occupied. Table 1 summarizes the crystal data and the structure refinement details. The three-dimensional structure along the *c*-direction, Figure 2(c), is formed by edge- and corner-shared (2/3 *RE* + 1/3 Eu)S_8 bicapped trigonal prisms that generate tetrahedral cavities occupied by Si to form the SiS_4 units.

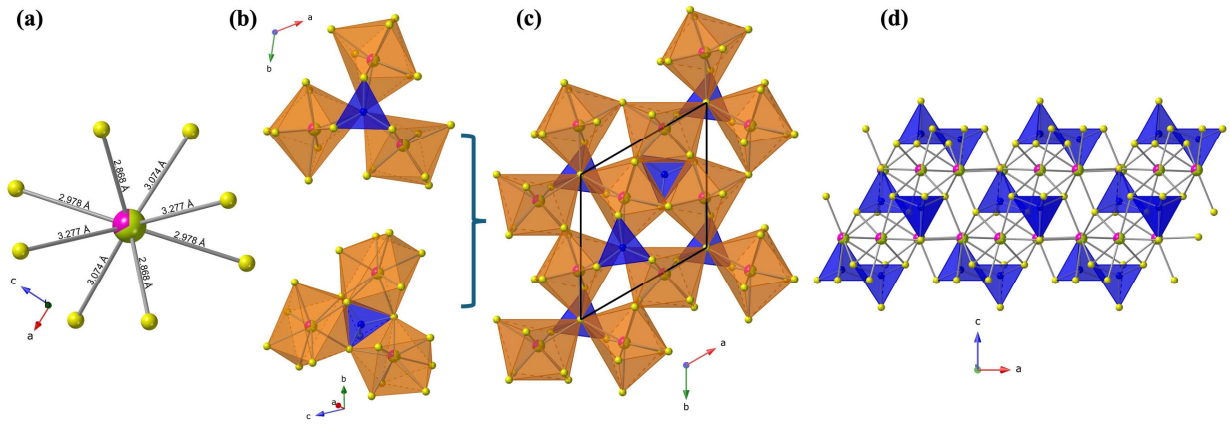

Figure 2: (a) The coordination environment of *RE*/EuS_8 in $RE_2EuSi_2S_8$, (b) repeating units of $RE_2EuSi_2S_8$, (c) unit cell structure of $RE_2EuSi_2S_8$ viewed along *c*-direction, and (d) along the *b*-direction. Rare earth orange, silicon dark blue, and sulfur yellow.

Magnetic Properties

Magnetic property measurements of $RE_2EuSi_2S_8$ (*RE* = Ce, Nd, and Gd) were studied on polycrystalline samples over the temperature range 2-300 K. Figure 3 shows the temperature dependent magnetic susceptibility from 2-300 K, and their magnetization vs field (M vs H) behavior from at 2K. The inverse susceptibility data for the 100-300 K range were fitted to the Curie-Weiss law, $\chi = C/(T-\theta_W)$, where χ is the molar susceptibility, *C* is the Curie constant, and θ_W is the Curie-Weiss temperature. The results of the fits are summarized in Table 2, where the negative θ_W values indicate the potential presence of antiferromagnetic interaction in $RE_2EuSi_2S_8$ (*RE* = Ce, Nd, and Gd).

Table 2: Summary of Magnetic Data for $RE_2EuSi_2S_8$ (*RE* = Ce, Nd, Gd)

compounds	effective magnetic moment μ_{eff} (μ_B/F. U)		θ_W (K)
	observed	calculated	
$Ce_2EuSi_2S_8$	7.46	8.69	-11.05
$Nd_2EuSi_2S_8$	8.53	9.45	-10.55
$Gd_2EuSi_2S_8$	13.55	13.71	-1.35

The observed effective magnetic moments per formula unit of $Ce_2EuSi_2S_8$, $Nd_2EuSi_2S_8$, and $Gd_2EuSi_2S_8$ are 7.46 μ_B, 8.53 μ_B, and 13.55 μ_B respectively, which are in reasonable agreement with the theoretical value of 8.69 μ_B, 9.45 μ_B, and 13.71 μ_B for the Ce, Nd, and Gd containing phases, respectively. The lower observed moments in the case of $Ce_2EuSi_2S_8$ and $Nd_2EuSi_2S_8$, is likely due to the presence of the minor impurities that impact the sample mass, Figure S1and S2. No difference was observed between the field-cooled and zero field-cooled data for these three compounds, and no evidence of long-range magnetic order was found. The M vs H plots (Figure 3, left side) exhibit evidence of magnetic saturation at high magnetic fields.

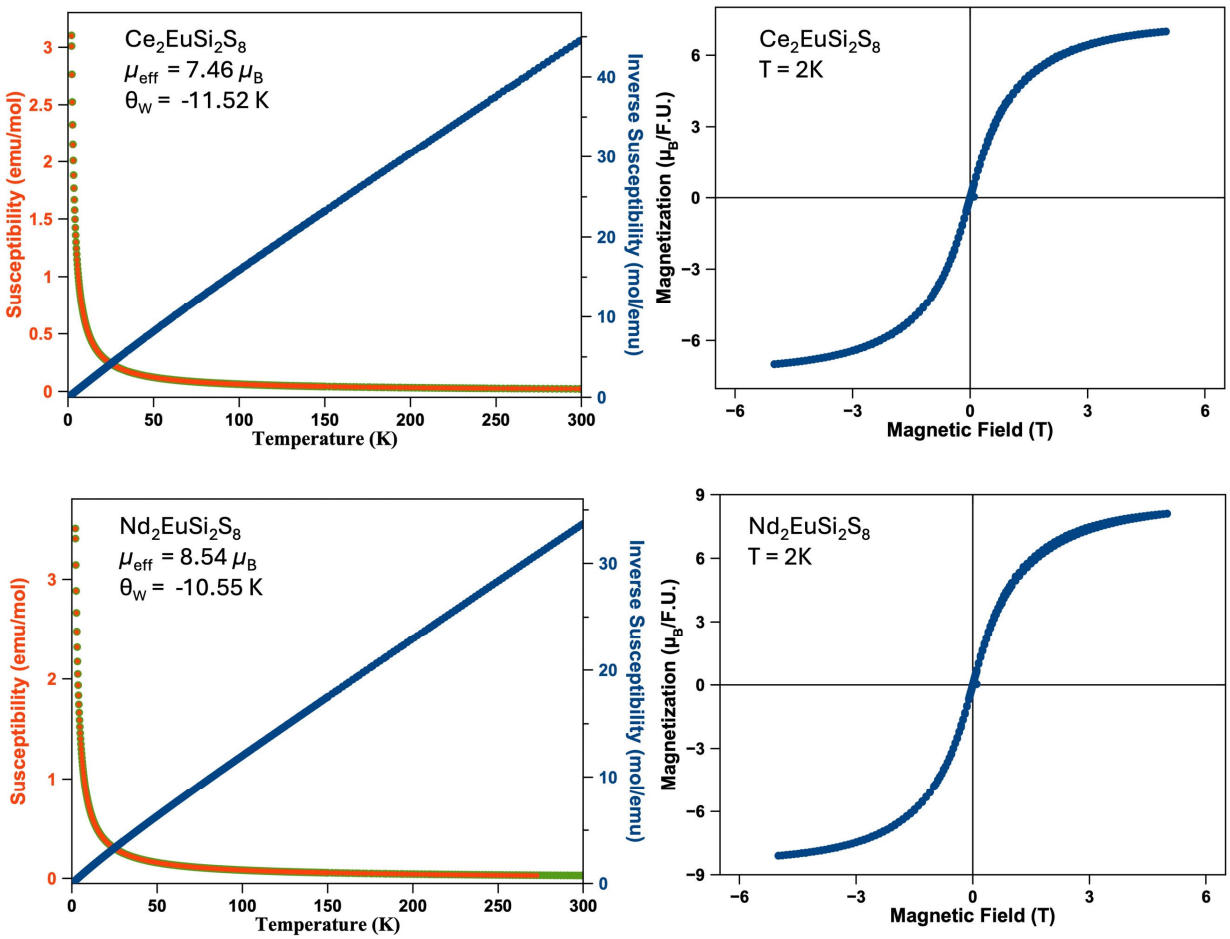

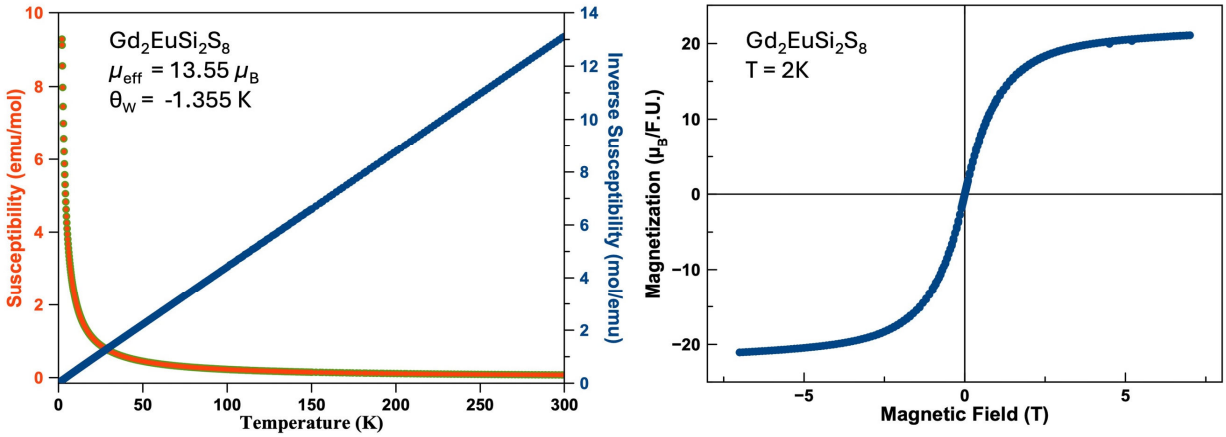

Figure 3: Magnetic data for $Ce_2EuSi_2S_8$, $Nd_2EuSi_2S_8$, and $Gd_2EuSi_2S_8$: (left) magnetic susceptibility and inverse magnetic susceptibility for the temperature range 2-300 K; (right) M vs H plot at 2K. Field-cooled (FC) data in red, Zero-field-cooled (ZFC) data are shown in green (the FC and ZFC data overlay), and the inverse susceptibility data in blue.

Thermogravimetric Analysis (TGA):

TGA was conducted on polycrystalline samples in a N_2 atmosphere up to 900 °C to evaluate their thermal stability. $Ce_2EuSi_2S_8$ (Figure 4a) began to lose weight rapidly from ~100-200 °C, after which point only a small additional weight loss was observed to 700 °C. It is possible that the low temperature weight loss was due moisture in the sample. In the case of $Nd_2EuSi_2S_8$ (see Figure 4b), only a small weight loss (less than 3%) was observed until around 600 °C, after which a pronounced drop occurred near 715 °C. $Sm_2EuSi_2S_8$ and $Gd_2EuSi_2S_8$ (Figure 4c, and 4d) showed almost identical mass-loss versus temperature profiles and lost less than 3% of their mass to 600 °C. PXRD analyses were carried out on the samples obtained after TGA, (see Figures S6-S9) indicating that the sample decomposed to primarily $EuLn_2S_4$ (Ln = Ce, Nd, Gd) and Sm_3S_4.

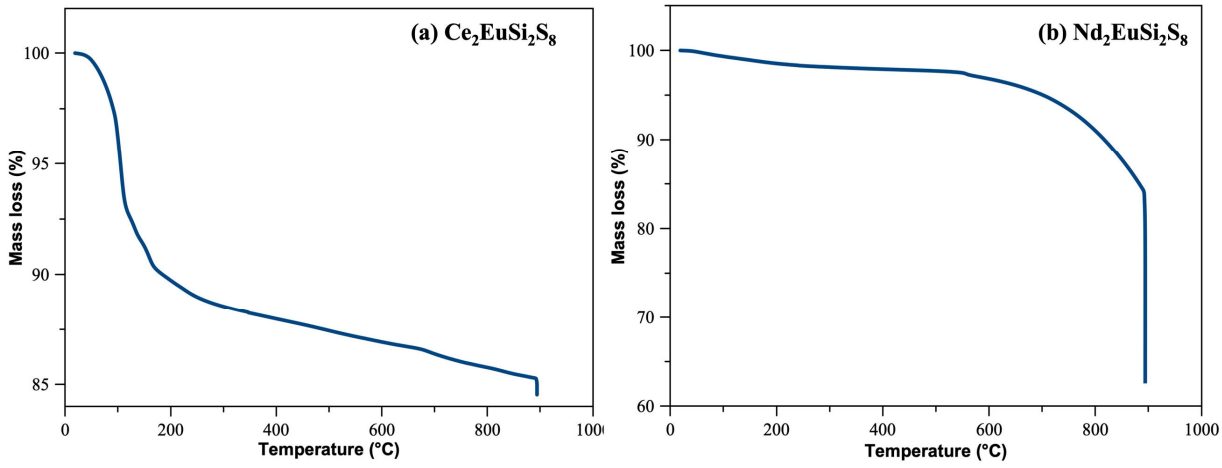

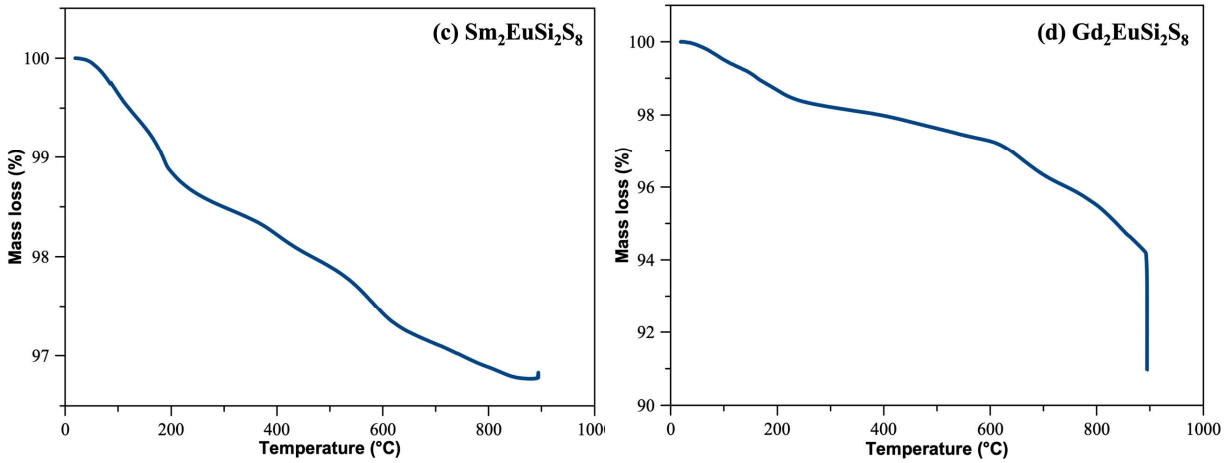

Figure 4: TGA plots showing the mass loss with temperature for (a) $Ce_2EuSi_2S_8$, (b) $Nd_2EuSi_2S_8$, (c) $Sm_2EuSi_2S_8$, and (d) $Gd_2EuSi_2S_8$ samples under N_2 flow.

UV-vis Diffuse Reflectance Spectroscopy

The optical properties of quaternary $RE_2EuSi_2S_8$ (*RE* = Ce, Nd, and Gd) were examined using polycrystalline powders. For $RE_2EuSi_2S_8$ (*RE* = Ce, Nd, and Gd), the diffuse reflectance data were converted to absorption using the Kubelka-Munk function, Figure 5(a, b, c), yielding estimated band gaps of 2.2(1) eV for $Ce_2EuSi_2S_8$, 1.8(1) eV for $Nd_2EuSi_2S_8$, and 1.7(1) eV for $Gd_2EuSi_2S_8$. The inset shows the wavelength vs absorption spectra. The UV-vis absorption spectrum of $Nd_2EuSi_2S_8$ exhibits multiple weak absorption peaks arising from the characteristic *f-f* electronic transitions of the Nd^{3+} cation. As shown in Figure 5(b), the broad features around 815 nm corresponds to the $^4F_{5/2}$ multiplet, a shoulder near 886 nm is assigned to the $^4F_{3/2}$ multiplet. Additional absorption peaks observed at 755 nm, 690 nm, 630 nm, and 590 nm correspond to the $^4F_{7/2}$, $^4F_{9/2}$, $^2H_{11/2}$, and $^4G_{5/2}$ multiplets, respectively. These transitions are consistent with previously reported optical absorption data for Nd^{3+} compounds. [22, 43]

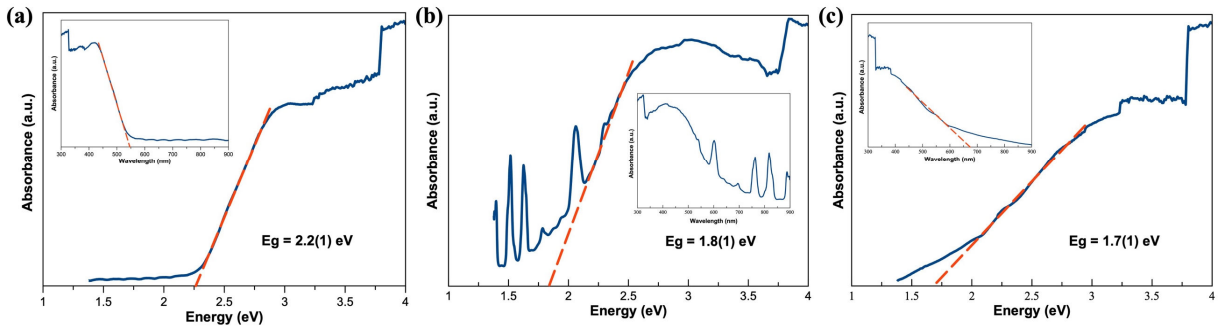

Figure 5: Optical absorption plot of polycrystalline (a) $Ce_2EuSi_2S_8$, (b) $Nd_2EuSi_2S_8$, and (c) $Gd_2EuSi_2S_8$ sample. The insets show the absorption wavelength vs absorption spectra.

Photoluminescence Emission Spectroscopy

Since the family of $RE_2ASi_2S_8$ (A = Ca, Sr, Ba) compounds exhibited interesting photoluminescence and scintillation activity,[13, 32, 33] we investigated the photoluminescence and scintillation behaviors of the $RE_2EuSi_2S_8$ (*RE* = Ce - Nd, Sm, Gd, Tb) series. All the samples were examined under UV light, where the luminescence behavior was observed in the case of $Ce_2EuSi_2S_8$, and $Tb_2EuSi_2S_8$. However, no scintillation response was detected when exposing the powders to Cu K_a radiation. The photoluminescence response was measured on single crystals using a 375 nm ultraviolet diode laser as the excitation source. For $Ce_2EuSi_2S_8$, Figure 6(a), a broad emission band was observed at 680 nm. In the case of $Tb_2EuSi_2S_8$, Figure 6(b), a broad emission band was observed at 583 nm. It is interesting that luminescence was observed only for these two phases. It is known that Eu^{2+} often exhibits broad band emission due to the $4f^6 5d \rightarrow 4f^7$ transition of the Eu^{2+} ion,[32, 44, 45] however, we might expect to observed this for all compositions. It is also possible that the specific rare earth element couples with the sulfur to generate luminescence. In the $ARE_2Si_2S_8$ (A = Ca, Sr; *RE* = La - Tb) series, luminescence was observed for the Ce, and Tb containing compositions. In these cases, however, broad emission bands were observed for the Ce containing compositions at ~525 nm and sharp f-f transitions were observed for the Tb containing composition. It is likely that in the case of $Ce_2EuSi_2S_8$ and $Tb_2EuSi_2S_8$ the presence of the Eu^{2+} changed the emission profile.

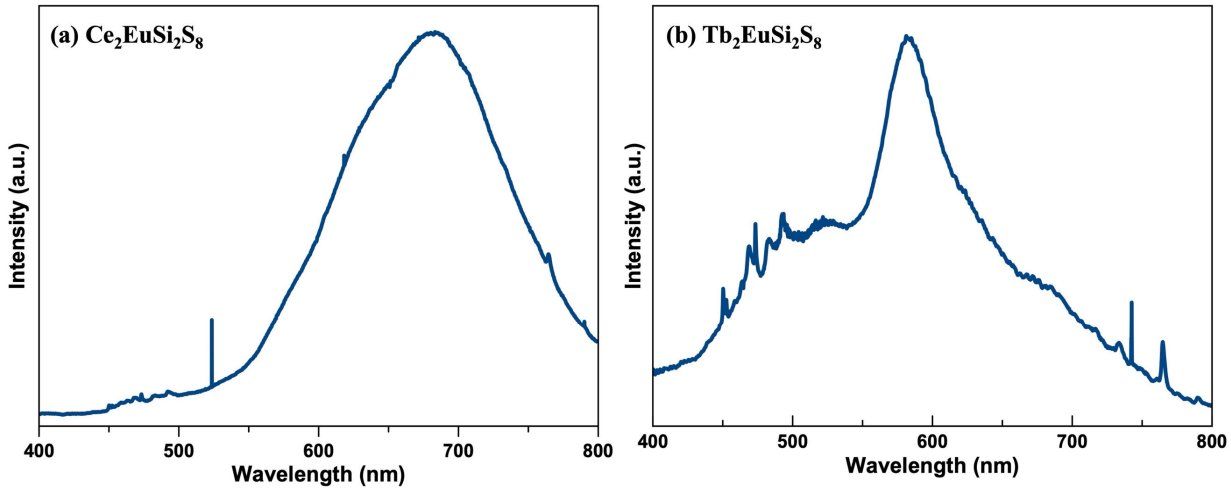

Figure 6: PL emission spectrum of (a) $Ce_2EuSi_2S_8$, and (b) $Tb_2EuSi_2S_8$ crystals at room temperature under 375 nm excitation.

Conclusion:

Six new quaternary rare-earth thiosilicates, $RE_2EuSi_2S_8$ (*RE* = Ce - Nd, Sm, Gd, Tb), crystallizing the *R*-3*c* space group, were successfully synthesized as single crystals, thereby expanding the $Eu_3(AsS_4)_2$ family of compounds. High quality single crystals were obtained by coupling the BCM method with the molten flux crystal growth. Single crystal X-ray diffraction was used to determine their crystal structures. Polycrystalline samples of $RE_2EuSi_2S_8$ (*RE* = Ce, Nd, Gd) were used for magnetic measurements, UV-visible diffuse reflectance, and photoluminescent measurements. Magnetic susceptibility measurements show paramagnetic behavior without any evidence of magnetic transition. UV-vis spectroscopy confirms the semiconducting nature of these materials. Broad emission bands were observed from the photoluminescence emission spectra for $Ce_2EuSi_2S_8$, and $Tb_2EuSi_2S_8$ at 680 nm and 583 nm respectively.

Notes

The authors declare no competing financial interest.

Associated Content

Supporting Information

Supporting information: PXRD patterns, EDS results, and post TGA PXRD patterns of the title compounds (PDF). This information is available free of charge at the website XXX.

The CCDC 2486368-2486373 entries encompass the supplementary crystallographic data associated with this paper. These data are accessible without charge through www.ccdc.cam.ac.uk/data_request/cif, or by sending a request via email to data_request@ccdc.cam.ac.uk, or by directly contacting The Cambridge Crystallographic Data Centre at 12 Union Road, Cambridge CB2 1EZ, UK; fax: +44 1223 336033.

ACKNOWLEDGMENTS

The authors gratefully acknowledge the support from the U.S. Department of Energy, Office of Basic Energy Sciences, Division of Materials Sciences and Engineering, under award

DE-SC0018739. Synthesis, structural characterization was conducted at the University of South Carolina.

References.

(1) Ishtiyak, M.; Panigrahi, G.; Jana, S.; Prakash, J.; Mesbah, A.; Malliakas, C. D.; Lebegue, S.; Ibers, J. A. Modulated Linear Tellurium Chains in Ba_3ScTe_5: Synthesis, Crystal Structure, Optical and Resistivity Studies, and Electronic Structure. *Inorg. Chem.* **2020**, *59*, 2434−2442.

(2) Messegee, Z. T.; Cho, J. S.; Craig, A. J.; Garlea, V. O.; Xin, Y.; Kang, C. J.; Proffen, T. E.; bhandari, H.; Kelly, J. C.; Ghimire, N. J.; Aitken, J. A.; Jang, J. I.; Tan, X. Multifunctional Cu_2TSiS_4 (T = Mn and Fe): Polar Semiconducting Antiferromagnets with Nonlinear Optical Properties. *Inorg. Chem.* **2022**, *62*, 530-542.

(3) Gan, Y.; Miao, N.; Lan, P.; Zhou, J.; Elliott, S. R.; Sun, Z. Robust Design of High-Performance Optoelectronic Chalcogenide Crystals from High-Throughput Computation. *J. Am. Chem. Soc.* **2022**, *144*, 5878−5886.

(4) Yu, Y.; Cagnoni, M.; Cojocaru-Mirédin, O.; Wuttig, M. Chalcogenide Thermoelectrics Empowered by an Unconventional Bonding Mechanism. *Adv. Funct. Mater.* **2020**, *30*, 1904862.

(5) King, A. A.; Breton, L. S.; Morrison, G.; Smith, M. D.; zur Loye, H.-C. Boron Chalcogen Mixture Method-Assisted Alkali Halide Flux Crystal Growth of an Extensive Family of Quaternary Rare Earth Transition-Metal Thiosilicates: Investigation of their Structures and Magnetic Properties. *Inorg. Chem.* **2023**, *62*, 18172-18178.

(6) Fabini, D. H.; Koerner, M.; Seshadri, R. Candidate Inorganic Photovoltaic Materials from Electronic Structure-Based Optical Absorption and Charge Transport Proxies. *Chem. Mater.* **2019**, *31*, 1561−1574.

(7) Mishra, N.; Dutt, V. G. V.; Arciniegas, M. P. Recent Progress on Metal Chalcogenide Semiconductor Tetrapod-Shaped Colloidal Nanocrystals and their Applications in Optoelectronics. *Chem. Mater.* **2019**, *31*, 9216−9242.

(8) Dey, T.; Mumbaraddi, D.; Firouzi-Haji, R.; Vrublevskiy, D.; Lin, Z.; meldrum, A.; mar, A. Rare-Earth Substitution of $La_3Si_2S_8I$ for Efficient and Color-Tunable Phosphor Converted White Light Emitting Diodes. *J. Am. Chem. Soc.* **2025**, *147*, 30347-30368.

(9) Anand, A.; Zaffalon, M. L.; Cova, F.; Pinchetti, V.; Khan, A. H.; carulli, F.; Brescia, R.; Meinardi, F.; moreels, I.; Brovelli, S. Optical and Scintillation Properties of Record-Efficiency CdTe Nanoplatelets toward Radiation Detection Applications. *Nano Lett.* **2022**, *22*, 8900-8907.

(10) Zhou, W.; Yao, W. D.; Zhang, Q.; Xue, H.; Guo, S. P. Introduction of Li into Ag-Based Noncentrosymmetric Sulfides for High-Performance Infrared Nonlinear Optical Materials. *Inorg. Chem.* **2021**, *60*, 5198−5205.

(11) Vecht, A.; Gibbons, C.; Davies, D.; Jing, X.; Marsh, P.; Ireland, T.; Silver, J.; Newport, A.; Barber, D. Engineering Phosphors for Field Emission Displays. *J. Vac. Sci. Technol. B*. **1999**, *17*, 750-757.

(12) Li, D.; Clark, B. L.; Keszler, D. A.; Keir, P.; Wager, J. F. Color Control in Sulfide Phosphors: Turning up the Light for Electroluminescent Displays. *Chem. Mater.* **2000**, *12*, 268-270.

(13) Lee, S. P.; Huang, C. H.; Chan, T. S.; Chen, T. M. New Ce^{3+}-Activated Thiosilicate Phosphor for LED Lighting Synthesis, Luminescence Studies, and Applications. *ACS Appl. Mater. Interfaces*. **2014**, *6*, 7260−7267.

(14) Berseneva, A. A.; Masachchi, L. W.; Jacobsohn, L. G.; zur Loye, H.-C. Tunable Salt-Inclusion Chalcogenides for Ion Exchange, Photoluminescence, and Scintillation. *Chem. Mater.* **2023**, *35*, 1417−1431.

(15) Haecke, J. E. V.; Smet, P. F.; Poelman, D. Luminescent Characterization of $CaAl_2S_4$: Eu Powder. *J Lumin.* **2007**, *126*, 508-514.

(16) Petrykin, V.; Kakihana, M. Direct Synthesis of $BaAl_2S_4$:Eu^{2+} Blue Emission Phosphor by One-Step Sulfurization of Highly Homogeneous Oxide Precursor Prepared Via a Solution-Based Method. *Chem. Mater.* **2008**, *20*, 5128-5130.

(17) Kumar, V.; Pitale, S. S.; Mishra, V.; Nagpure, I. M.; Biggs, M. M.; Ntwaeaborwa, O. M.; Swart, H. C. Luminescence Investigations of Ce^{3+} Doped CaS Nanophosphors. *J. Alloys Compd.* **2010**, *492*, L8-L12.

(18) Liang, H.; Yang, G.; Bai, S.; Li, C.; Li, X.; Wang, Y.; Huang, J.; Ji, J.; Zhu, Y. Efficient and Tunable Photoluminescence for Terbium-Doped Rare-Earth-based Cs_2NaYCl_6 Double Perovskite. *Opt. Lett.* **2022**, *47*, 5176-5179.

(19) Naresh, V.; Cha, P. R.; Lee, N. $Cs_2NaGdCl_6$:Tb^{3+}─a Highly Luminescent Rare-Earth Double Perovskite Scintillator for Low-Dose X-Ray Detection and Imaging. *ACS Appl. Mater. Interfaces*. **2024**, *16*, 19068-19080.

(20) Wu, L. M.; Seo, D. K. New Solid− Gas Metathetical Synthesis of Binary Metal Polysulfides and Sulfides at Intermediate Temperatures: Utilization of Boron Sulfides. *J. Am. Chem. Soc.* **2004**, *126*, 4676-4681.

(21) Berseneva, A. A.; Klepov, V. V.; Kashem, H. B.; Maksimova, A. A.; Morrison, G.; Wright, J.; Schaeperkoetter, J.; Misture, S. T.; zur Loye, H.-C. Rare Bird: U^{+5} in Uranium Chalcogenides. *Chem. Mater.* **2024**, *36*, 7988-8001.

(22) Kashem, H. B.; Panigrahi, G.; Morrison, G.; Gabilondo, E. A.; Halasyamani, P. S.; Wisesa, P.; Besmann, T. M.; zur Loye, H.-C. Crystal Growth of Quaternary Rare Earth Selenosilicates By Using the Flux-Assisted Boron Chalcogen Mixture Method: Investigation of Their Magnetic and Optical Properties. *Cryst. Growth Des.* **2025**, *25*, 3767-3775.

(23) Panigrahi, G.; Kashem, H. B.; Morrison, G.; zur Loye, H.-C. Synthesis of a Series of Rare-Earth-Based Multi-Anion Chalcogenide Iodides $Re_3Si_2Se_xS_{8-x}I$ (RE= La, Ce, Pr, and Nd) Using the Flux-Assisted Boron–Chalcogen Mixture Method. *Dalton Trans.* **2025**, *54*, 6252-6260.

(24) Ma, N.; Li, Y. Y.; Chen, L.; Wu, L. M. α-$CsCu_5Se_3$: Discovery of a Low-Cost Bulk Selenide with High Thermoelectric Performance. *J. Am. Chem. Soc.* **2020**, *142*, 5293-5303.

(25) King, A. A.; Breton, L. S.; Morrison, G.; Smith, M. D.; zur Loye, H.-C. Boron Chalcogen Mixture Method-Assisted Alkali Halide Flux Crystal Growth of an Extensive Family of Quaternary Rare Earth Transition-Metal Thiosilicates: Investigation of their Structures and Magnetic Properties. *Inorg. Chem.* **2023**, *62*, 18172-18178.

(26) O'Donnell, S.; Leahy, I. A.; Jana, S.; Gabilondo, E. A.; Halasyamani, P. S.; Maggard, P. A.; Smaha, R. W. Magnetic Properties and Large Second-Harmonic Generation Response of a Chiral Ternary Chalcogenide: Eu_2sise_4. *Chem. Mater.* **2025**, *37*, 5036-5042.

(27) Usman, M.; Smith, M. D.; Morrison, G.; Klepov, V. V.; Zhang, W.; Halasyamani, P. S.; zur Loye, H.-C. Molten Alkali Halide Flux Growth of an Extensive Family of Noncentrosymmetric Rare Earth Sulfides: Structure and Magnetic and Optical (SHG) Properties. *Inorg. Chem.* **2019**, *58*, 8541−8550.

(28) Kashem, H. B.; Tisdale, H. B.; zur Loye, H.-C. Structural Investigation of Six Quinary Sulfides Synthesized via the Flux-Assisted Boron-Chalcogen Mixture (BCM) Method: Eu^{2+} Containing Members of the RE_3MTQ_7 (M and T = Transition or Main Group MEtals, Q = chalcogens) Family. *Inorg. Chem.* **2025**, In print.

(29) Bera, T. K.; Iyer, R. G.; Malliakas, C. D.; Kanatzidis, M. G. $Eu_3(AsS_4)_2$ and $A_xEu_{3-y}As_{5-z}S_{10}$ (A = Li, Na): Compounds with Simple and Complex Thioarsenate Building Blocks. *Inorg. Chem.* **2007**, *46*, 8466-8468.

(30) Gulay, L. D.; Daszkiewicz, M.; Ruda, I. P.; marchuk, O. V. $La_2Pb(SiS_4)_2$. *Acta. Cryst.* **2010**, *C66*, i19-i21.

(31) Daszkiewicz, M.; Marchuk, O. V.; Gulay, L. D.; Kaczorowski, D. Crystal Structures and Magnetic Properties of $R_2PbSi_2S_8$ (R= Y, Ce, Pr, Nd, Sm, Gd, Tb, Dy, Ho), $R_2PbSi_2Se_8$ (R= La, Ce, Pr, Nd, Sm, Gd) and $R_2PbGe_2S_8$ (R = Ce, Pr) Compounds. *J. Alloys Compd.* **2012**, *519*, 85-91.

(32) Lee, S. P.; Chan, T. S.; Chen, T. M. Novel Reddish-Orange-Emitting $BaLa_2Si_2S_8:Eu^{2+}$ Thiosilicate Phosphor for Led Lighting. *ACS Appl. Mater. Interfaces*. **2015**, *7*, 40-44.

(33) Panigrahi, G.; Berseneva, A. A.; Morrison, G.; King, A. A.; Conner, R. L.; Jacobsohn, L. G.; zur Loye, H.-C. Crystal Growth of Quaternary $AkRE_2Si_2S_8$ (Ak = Ca and Sr; RE = La–Tb) Thiosilicates using Flux-Assisted Boron Chalcogen Mixture Method: Exploring X-Ray Scintillation, Luminescence, and Magnetic Properties. *Inorg. Chem.* **2024**, *63*, 12849−12857.

(34) Muhit, M. A. A.; Wechsler, S. C.; Bare, Z. J. L.; Sturgill, C. J.; Keerthisinghe, N.; Grasser, M. A.; Morrison, G.; Sutton, C.; Stefik, M.; zur Loye, H.-C. Comparison of Lithium Diffusion in Isostructural $Ta_{12}MoO_{33}$ and $Nb_{12}MoO_{33}$: Experimental and Computational Insights from Single Crystals. *Chem. Mater.* **2024**, *36*, 10626-10639.

(35) Muhit, M. A. A.; Maksimova, A. A.; Wechsler, S. C.; Kashem, H. B.; Panigrahi, G.; Morrison, G.; Stefik, M.; zur Loye, H.-C. Crystal Growth, Thermal, Optical, Magnetic and Electrochemical Properties of $Mo_2Ta_2O_{11}$. *Solid State Sci.* **2025**, *165*, 107951.

(36) Krause, L.; Herbst-Irmer, R.; Sheldric, G. M.; Stalke, D. Comparison of Silver and Molybdenum Microfocus X-Ray Sources for Single-Crystal Structure Determination. *J. Appl. Crystallogr.* **2015**, *48*, 3-10.

(37) Hübschle, C. B.; Sheldrick, G. M.; Dittrich, B. Shelxle: A Qt Graphical User Interface for SHELXL. *J. Appl. Cryst.* **2011**, *44*, 1281-1284.

(38) Dolomanov, O. V.; Bourhis, L. J.; Gildea, R. J.; Howard, J. A.; Puschmann, H. Olex2: A Complete Structure Solution, Refinement and Analysis Program. *J. Appl. Cryst. (***2009**, *42*, 339-341.

(39) Morrison, G.; zur Loye, H.-C. Simple Correction for the Sample Shape and Radial Offset Effects on Squid Magnetometers: Magnetic Measurements on Ln_2O_3 (Ln= Gd, Dy, Er) Standards. *J. Solid State Chem.* **2015**, *221*, 334-337.

(40) Kubelka, P. Ein Beitrag zur Optik der Farbanstriche. *Z. Technol. Phys.* **1931**, *12*, 593.

(41) Klepov, V. V.; Juillerat, C. A.; Pace, K. A.; Morrison, G.; zur Loye, H.-C. “Soft” Alkali Bromide and Iodide Fluxes for Crystal Growth. *Front. Chem.* **2020**, *8*, 518.

(42) Daszkiewicz, M.; Marchuk, O. V.; Gulay, L. D.; Kaczorowski, D. Crystal Structures and Magnetic Properties of $R_2PbSi_2S_8$ (R= Y, Ce, Pr, Nd, Sm, Gd, Tb, Dy, Ho), $R_2PbSi_2Se_8$ (R= La, Ce, Pr, Nd, Sm, Gd) and $R_2PbGe_2S_8$ (R= Ce, Pr) Compounds. *J. Alloys Compd.* **2012**, *519*, 85-91.

(43) Jiang, Z.; Yang, J.; Dai, S. Optical Spectroscopy and Gain Properties of Nd^{3+} - Doped Oxide Glasses. *JOSA B*. **2004**, *21*, 739-743.

(44) Kim, H. S.; Machida, K.; Horikawa, T.; Hanzawa, H. Luminescence Properties of $CaAlSiN_3$: Eu^{2+} Phosphor Prepared by Direct-Nitriding Method Using Fine Metal Hydride Powders. *J. Alloys Compd.* **2015**, *633*, 97-103.

(45) Lien, N. T. Q.; Trac, N. N.; Do, P. V.; Tuyen, H. V. Judd-Ofelt Analysis of Eu^{3+} and Adjustable Emission in Eu^{3+}/Eu^{2+} Co-Doped Sodium Aluminosilicate Glasses. *J. Phys. Chem. Solids*. **2022**, *164*, 110637.

For Table of Contents Use Only

Crystal Growth of Quaternary $RE_2EuSi_2S_8$ (*RE* = Ce - Nd, Sm, Gd, Tb) Using Flux-Assisted Boron Chalcogen Mixture (BCM) Method: Investigation of Magnetic and Luminescence Properties

Habiba Binte Kashem, Hope Smith, Md Abdullah Al Muhit, and Hans-Conrad zur Loye*

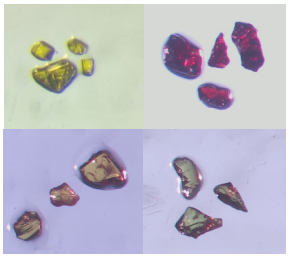

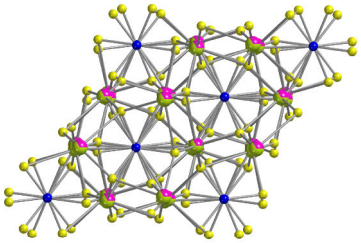

Synopsis:

Six new quaternary rare-earth containing thiosilicates, $RE_2EuSi_2S_8$ (*RE* = Ce - Nd, Sm, Gd, Tb) were obtained via the flux-assisted boron chalcogen mixture (BCM) method. Magnetic data of $RE_2EuSi_2S_8$ (*RE* = Ce, Nd, and Gd) showed paramagnetic behavior with negative Weiss constants. Photoluminescence measurements were studied on $Ce_2EuSi_2S_8$, and $Tb_2EuSi_2S_8$ single crystals.